*Journal of Earth Science*, *Vol. 27*, *No. 1*, *p. 098–109*, *February 2016* *ISSN 1674-487X*
*Printed in China*
DOI: 10.1007/s12583-016-0632-5

# Hyporheic Zone Flow Disruption from Channel Linings: Implications for the Hydrology and Geochemistry of an Urban Stream, St. Louis, Missouri, USA

**Elizabeth A. Hasenmueller***, **Heather K. Robinson**
*Department of Earth and Atmospheric Sciences*, *Saint Louis University*, *St. Louis MO* 63108, *USA*

**ABSTRACT: Cement channel linings in an urban stream in St. Louis, Missouri increase event water contributions during flooding, shorten transport times, and magnify geochemical variability on both short and seasonal timescales due to disruption of hyporheic flowpaths. Detailed analyses of water isotopes, major and trace elements, and in situ water quality data for an individual flood event reveal that baseflow contributions rise by 8% only 320 m downstream of the point where this particular channel changes from cement-lined to unlined. However, additional hydrograph separations indicate baseflow contributions are variable and can be much higher (average baseflow increase is 16%). Stream electrical conductivity (EC) and solute concentrations in the lined reach were up to 25% lower during peak flow than in the unlined channel, indicating a greater event flow fraction. In contrast, during low flow, stream EC and solute concentrations in the lined reach were up to 30% higher due to the restricted inflow of more dilute groundwater. Over longer timescales, EC, solute concentrations, turbidity, and bacterial loads decrease downstream signifying increasing contributions of dilute baseflow. The decreased connectivity of surface waters and groundwaters along the hyporheic zone in lined channels increases the hydrologic and geochemical variability of urban streams.**
**KEY WORDS: stream channel linings, hyporheic zone, groundwater-surface water interactions, flood hydrograph, urban geochemistry, urban streams.**

## 0 INTRODUCTION

Urban stream degradation is exacerbated by common river engineering measures such as the lining and straightening of channels. When stream channels are lined with impervious materials like concrete, there is substantial hydrologic disruption of the hyporheic zone, the region of streambed sediments in which stream water and local groundwater mix. Moreover, removal of meanders and replacement of natural riverbeds with low friction concrete increases flow velocity and erosive capacity (Hancock, 2002). Channel straightening also removes riffle and pool sequences, modifies streambed sediment grain size distributions, and reduces in-stream cover, rendering streams uninhabitable for certain fish species (Lau et al., 2006).

Hyporheic zone flow is determined by hydraulic conductivity and hydraulic gradients, so it varies spatially with geomorphic features and local particle size distribution, as well as temporally with discharge (Rivett et al., 2011; Ryan et al., 2010; Boulton et al., 1998). In urban settings, reduced groundwater recharge and modified flood dynamics alter hyporheic zone extent and flowpaths through changes in water table levels and channel morphology (Hancock, 2002; Wondzell and Swanson, 1999). Disruption of natural hyporheic flow patterns can affect habitat suitability for invertebrates and can alter the dynamics of streambed biogeochemical processes such as nitrification and denitrification (Bukaveckas, 2007; Hinkle et al., 2001; Boulton et al., 1998).

In terms of hyporheic zone processes, concrete-lined channels should behave similarly to bedrock channels because the streambed consists of impermeable material (Vaughn, 1990). In bedrock channels, hyporheic zone flow is negligible except in cases of localized alluvial deposits or fissures in the bedrock (Buffington and Tonina, 2009; White, 1993). Gooseff et al. (2005) showed a more than 3 200% increase in water residence time between a bedrock and alluvial channel in Oregon and attributed the difference to the absence of hyporheic flow in the bedrock channel.

We assert that lined channels, like bedrock channels, preclude hyporheic flow entirely and that even small stretches of more natural, unlined channel could substantially and rapidly increase baseflow along the hyporheic zone of urban streams. Surprisingly, to our knowledge no studies have specifically addressed the hydrologic and geochemical consequences of stream channel lining. To address our hypothesis, we monitored water discharge and geochemistry at three sites along an urban stream that features similar land use throughout the watershed, but includes both cement-lined and more natural, unlined reaches of streambed. We show that channel linings re-

*Corresponding author: hasenmuellerea@slu.edu


Manuscript received January 27, 2015.
Manuscript accepted March 18, 2015.

Hasenmueller, E. A., Robinson, H. K., 2016. Hyporheic Zone Flow Disruption from Channel Linings: Implications for the Hydrology and Geochemistry of an Urban Stream, St. Louis, Missouri, USA. *Journal of Earth Science*, 27(1): 98–109. doi: 10.1007/s12583-016-0632-5. http://en.earth-science.net

strict the exchange of hyporheic waters, and result in reduced water quality and baseflow contributions both during flooding events and seasonally.

## 1 STUDY SITES

Three sites in the River des Peres watershed (Fig. 1) were monitored from 2009–2011 to investigate the effects of cement channel linings on surface water hydrology and geochemistry. The River des Peres is a highly degraded river in St. Louis, Missouri, that extends ~30 km before discharging into the Mississippi River. The 295 $km^2$ watershed has >90% urban land coverage (U.S. Geological Survey; USGS, 2015a; Fig. 1) and a population density of 1 990 people per $km^2$ (U.S. Census, 2010). This small river is located in a temperate, humid region with abundant rainfall (i.e., 97 $cm \cdot yr^{-1}$; NOAA, 2015). Average monthly rainfall is 8.4±2.8 cm (NOAA, 2015); regional runoff is variable, being about 4.5 times higher during March to May than in August to October (USGS, 2015b). Local bedrock in the catchment is predominantly Mississippian limestone in the southwest and Pennsylvanian shale in the northeast overlain by Quaternary loess soils (Harrison, 1997; Lutzen and Rockaway Jr., 1989).

We focused our monitoring efforts on the Upper River des Peres, which drains portions of a major highway (Interstate 170), commercial zones, municipal parks, and residential areas; land use and impervious surface area are similar throughout the study area (Table 1; Fig. 1). Large portions of the stream are housed in culverts and cement-lined channels. As described in detail elsewhere (Hasenmueller and Criss, 2013a; Hasenmueller, 2011), the upper two monitoring sites are along the "southwest branch," a first order tributary to the Upper River des Peres.

The most upstream site (RDP-1; Fig. 1) is located in a plunge pool just below a small bridge at the terminus of a cement-walled channel (2.2 km long) that drains an area of 2.9 $km^2$. Discharge at this site fluctuates rapidly during rainfall events, though transient temperature variations are attenuated

**Table 1** Basin characteristics, flooding response behavior, and average seasonal values of various water quality parameters

| | | RDP-1 | RDP-2 | RDP-3 |
|---|---|---|---|---|
| Basin characteristics | Drainage area ($km^2$) | 2.9 | 3.1 | 23.8 |
| | Impervious surface area (%) | 37.9 | 37.8 | 44.3 |
| | Road length (km) | 34.2 | 36.6 | 257.6 |
| | Upstream reach length (km) | 2.2 | 0.32 | 4.4 |
| | Upstream lined channel (%) | 100 | 0 | 8.9 |
| | Discharge ($m^3 \cdot s^{-1}$) | 0.07 | ~0.07 | 0.30 |
| | Peak discharge ($m^3 \cdot s^{-1}$) | 9.4 | ~9.4 | 143.0 |
| Flooding response[a] | Average baseflow (%) | 22 | 38 | 41 |
| | Baseflow (%) | 23 | 31 | 62 |
| | Minimum baseflow (%) | 0 | 8 | 17 |
| | Observed lag time (hours)[b] | 1.5 | NA | 2.0 |
| | Return to baseflow (hours)[c] | 22 | NA | 27 |
| | Peak flow ($m^3 \cdot s^{-1}$) | 1.25 | NA | 8.63 |
| | Baseflow $\delta^{18}O$ and $\delta^2H$ (‰) | -7.6; -51 | -7.0; -49 | -7.3; -53 |
| | Maximum $\delta^{18}O$ and $\delta^2H$ (‰) | -4.4; -26 | -4.6; -27 | -6.8; -43 |
| | Minimum $\delta^{18}O$ and $\delta^2H$ (‰) | -9.0; -59 | -8.4; -57 | -8.5; -56 |
| | Baseflow EC ($\mu S \cdot cm^{-1}$) | 1 654 | 1 517 | 1 427 |
| | Peak flow EC ($\mu S \cdot cm^{-1}$) | 214 | 265 | 383 |
| Seasonal response | Temperature (ºC) | 13.9 | 14.3 | 14.6 |
| | EC ($\mu S \cdot cm^{-1}$) | 1 478 | 1 389 | 1 239 |
| | DO (%) | 74.4 | 79.3 | 83.4 |
| | pH | 8.20 | 8.12 | 8.20 |
| | Turbidity (NTU) | 17.3 | 16.9 | 14.2 |
| | $Cl^-$ ($mg \cdot L^{-1}$) | 294.2 | 291.9 | 267.8 |
| | $NH_4^+$-N ($mg \cdot L^{-1}$) | 0.66 | 0.42 | 0.39 |
| | $NO_3^-$-N ($mg \cdot L^{-1}$) | 1.0 | 1.2 | 0.8 |
| | Total $PO_4^{3-}$ ($mg \cdot L^{-1}$)[d] | 0.64 | 0.50 | 0.27 |
| | *E. coli* (cfu·100 $mL^{-1}$)[e] | 1 717 | 1 438 | 1 410 |
| | Off-scale *E. coli* measurements (%)[f] | 48 | 43 | 43 |

[a] All flooding response parameters are for the April 2–3, 2010 event except average baseflow (average of 10 storm events from 2009–2010); [b] lag time from the second precipitation event centroid to peak flow; [c] time difference between the second precipitation event centroid and return to discharge conditions representative of baseflow; [d] based on 4 measurements per site, which were made from June to August, 2010; [e] the detection limit (i.e., 2 420 cfu·100 $mL^{-1}$) was used to calculate a minimum average *E. coli* level when measurements were off-scale; [f] percent of *E. coli* measurements that were off-scale; NA. not available.

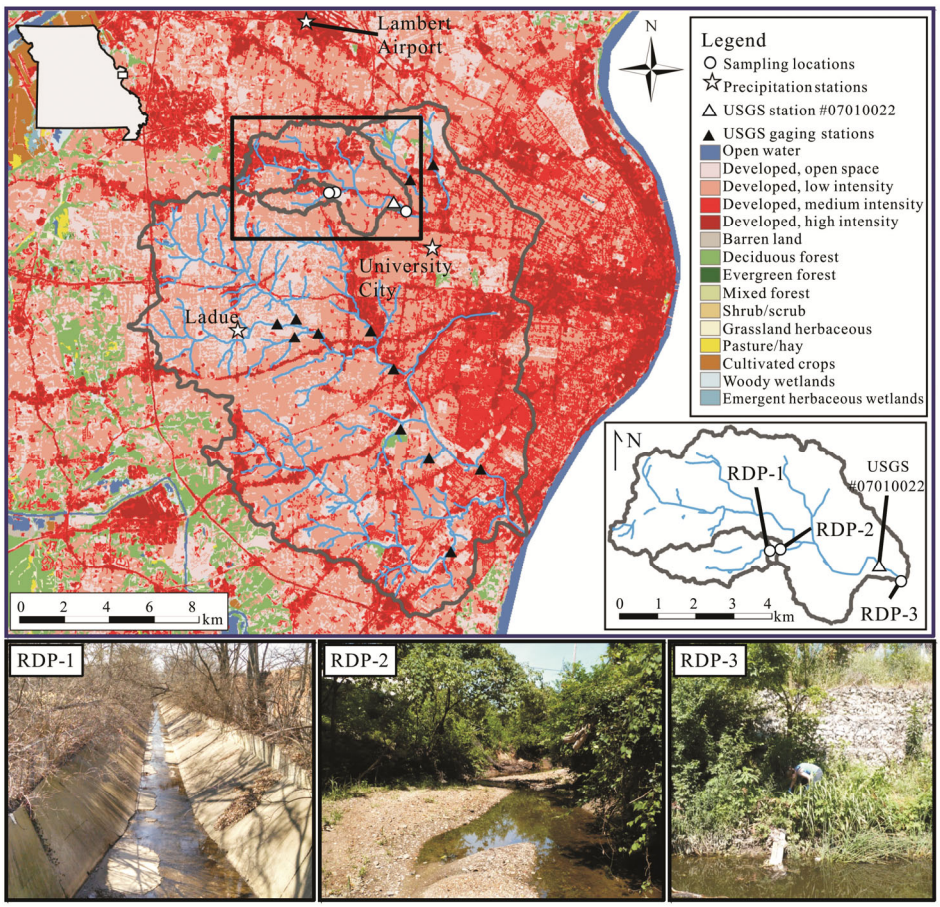


**Figure 1.** Site map (top) for the sampling locations in the River des Peres watershed (open circles), USGS gauging stations (closed triangles), including station #07010022 near RDP-3 (open triangle), and precipitation monitoring locations (open stars). Watershed boundaries are delineated on a land use/land cover map of east-central Missouri (2011 National Land Cover Database; USGS, 2015a). The inset shows the sampling locations (i.e., RDP-1, RDP-2, and RDP-3) in the Upper River des Peres subwatershed. Note that portions of the Upper River des Peres and its tributaries are piped underground (i.e., gaps in stream reaches). Photographs of each sampling site (bottom) demonstrate the typical level of channel lining along the study reach.

because of the ~1 m deep plunge pool. One combined sewer overflow (CSO) is located upstream (MSD, 2015).

Downstream of RDP-1, the southwest branch immediately enters a wooded area in Ruth Park where the channel features a more natural, but erosionally entrenched, streambed. Site RDP-2 (3.1 km$^2$; Fig. 1) is located only 320 m downstream of RDP-1; this reach contains partly vegetated banks and no CSOs. A golf course, mulching operation, and commercial area between the two sites contribute surface runoff intermittently. The mulching operation produces only small volumes of leachate (up to 30 L/s) that discharge directly into the stream channel.

Finally, site RDP-3 (23.8 km$^2$; Fig. 1) is located in Heman Park about 4.4 km downstream of RDP-2 along the Upper River des Peres, now a third order stream that receives flow from the southwest branch, an unnamed tributary, and the main stem. The reach between RDP-2 and RDP-3 is mostly unlined streambed (except for a 390 m concrete-lined channel segment) and features partially vegetated banks. However, above their confluence with the southwest branch, the main stem and unnamed tributary have ~2.2 km of lined channel. A USGS gaging station (#07010022; USGS, 2015b) is located 800 m upstream of RDP-3 (Fig. 1). There are 16 CSOs above this site (MSD, 2015).

## 2 METHODS

We combined biweekly field sampling, high frequency sampling during storm perturbations, continuous in situ monitoring, and spatial surveys of stream geochemistry to understand how channel linings disrupt hyporheic flow in the Upper River des Peres. To this end, we examined the stream's hydrologic and geochemical response to flooding events and daily fluctuations as well as its long-term seasonal behavior along lined and unlined reaches. The complete set of analytical data collected during this project is too large for tabulation here, but selected data and statistical summaries are presented in Tables 1 and S1. The entire analytical dataset can be found in Hasenmueller (2011).

During biweekly field visits (i.e., March 2009 to July 2011), point measurements of temperature, electrical conductivity (EC; measured as specific conductance), dissolved oxygen (DO), pH, and turbidity were measured with handheld meters and grab samples were collected for laboratory analysis. We conducted two spatial surveys of stream geochemistry along the unlined reach between RDP-1 and RDP-2 using the handheld water quality meters. Spatial measurements were taken during low flow on November 12, 2014, before winter road salt applications, and March 11, 2015, immediately fol-

lowing the salting season. In situ continuous monitoring devices (i.e., YSI 6600 V2 sondes) were deployed from March to September 2010 at RDP-1, RDP-2, and RDP-3. These instruments continuously measured (5-minute data intervals) a suite of water quality parameters, including temperature, EC, DO, pH, turbidity, $Cl^-$, $NH_4^+$-N, and $NO_3^-$-N. In addition, automatic sampling devices (i.e., ISCO models 3700 and 6712) were used to collect physical samples at each monitoring site during floods; generally 10–60 samples were obtained to characterize these events. The RDP-1 autosampler was equipped with an acoustic stage recorder (ISCO 710 Ultra Sonic Flow Module), which was located in a culvert 2 m upstream of RDP-1. Stage data were measured at 5-minute intervals, and discharge was determined from monitored stages using well-known empirical relationships (e.g., Fetter, 2001). Discharge at RDP-1 was used to approximate discharge at RDP-2, though we recognize that increased basin area and groundwater discharge or recharge could modify flow volumes. At RDP-3, discharge data was provided by USGS gaging station #07010022 located only 800 m upstream (USGS, 2015b).

Rain water samples were collected for isotopic analysis to determine the proportion of "new" water contributed to stream flow during flooding for each sampling site. Rainfall amounts and chemistry were characterized with two rain gauges in University City and Ladue, Missouri; both gauges were within 8 km of the sampling sites (Fig. 1). Rainfall samples included total rainfall during a storm event as well as time series samples every 4 to 6 h. For better temporal resolution during precipitation events, we also utilized hourly precipitation data monitored by National Weather Service (NWS) at Lambert-St. Louis International Airport, only 9 km away (NOAA, 2015; Fig. 1).

We separated field samples into subsamples for geochemical analyses. Subsamples for major and trace elemental analyses were field-filtered (0.45 μm acetate filters) and field-acidified (trace metal grade $HNO_3$). Major element concentrations were measured with an Inductively Coupled Plasma Optical Emissions Spectrometer (ICP-OES; Perkin-Elmer Optima 7300DV ICP-OES) in accordance with the techniques outlined in U.S. Environmental Protection Agency (USEPA) Method 200.7 (USEPA, 1990). Trace elements were analyzed with an Inductively Coupled Plasma Mass Spectrometer (Perkin-Elmer ELAN DRC II ICP-MS) using USEPA Method 200.8 (USEPA, 1994). Instrument operation and data processing were completed with the WinLab32™ (ICP-OES) and ELAN® (ICP-MS) software packages. Blanks, reference standards (Sigma-Aldrich TraceCERT® and Perkin-Elmer Pure Plus), and duplicate and triplicate samples were also analyzed to check the precision and accuracy of analytical procedures; laboratory accuracy was ±5%. Additional subsamples for major ions ($Cl^-$, $NH_4^+$-N, $NO_3^-$-N, and total P as $PO_4^{3-}$) were collected in pre-cleaned high density polyethylene (HDPE; $Cl^-$, $NH_4^+$-N, $NO_3^-$-N) or glass (total P) bottles. Concentrations were determined using USEPA-approved techniques (Hach, 2005a, b, c, d, e, respectively).

Additional stream water samples were collected in pre-cleaned, autoclaved HDPE bottles to measure *Escherichia coli* (*E. coli*) levels. We used the IDEXX Colilert reagent and 97-well Quanti-Tray® to enumerate colonies; all labware for *E. coli* analyses was autoclaved. This USEPA approved method has a most probable number range limit of 1 to 2 420 cfu 100 $mL^{-1}$.

Stable isotopes of O and H for stream waters were measured with an isotope ratio mass spectrometer (IR-MS; Finnigan MAT 252) using standard methods (see Hasenmueller, 2011) and are reported in the usual manner as $\delta^{18}O$ and $\delta^2H$ values relative to V-SMOW; precision is respectively ±0.1‰ and ±1.0‰. In the following discussion, $\delta^{18}O$ and $\delta^2H$ values will always be listed in that order. Isotope results were used to calculate the relative contributions of baseflow (through the hyporheic zone into the channel) and event water (from recent rainfall) to stream flow during flooding (i.e., hydrograph separations; Sklash and Farvolden, 1979). The relationship for two end-member mixing takes the form of Eq. (1)

$$Q_tC_t=Q_bC_b+Q_eC_e \tag{1}$$

where $Q$ is the discharge, $C$ is the isotopic $\delta$-value, and the subscripts represent the total ($t$), baseflow ($b$), or event water ($e$) discharge or isotopic $\delta$-value. This relationship can be solved to obtain the fraction of discharge derived from baseflow ($X_b$), which is equal to $Q_b/Q_t$. The result is Eq. (2),

$$X_b = \frac{C_i - C_e}{C_b - C_e} \tag{2}$$

where $C_i$ is isotopic $\delta$-value in the stream at any given time during the flood. For our study, baseflow was defined by samples with (1) isotope values close to the weighted, long-term average of local meteoric precipitation (i.e., -7.0‰ and -45‰; see Criss, 1999), (2) EC values near the seasonal average for the stream, and (3) low stage. In contrast, event water features relatively low EC compared to baseflow, has variable isotopic composition, and occurs during high flow.

Statistical analyses included Pearson correlation coefficients and paired t-tests that were calculated using Microsoft Excel. For the Pearson correlation, an indicative limit of ±0.65 (i.e., $R^2$>0.4) was proposed as a reasonable choice for roughly separating the relevant correlations.

## 3 RESULTS

### 3.1 Response to a Flooding Event

We collected samples for a total of 10 flooding events at the three Upper River des Peres sites over the monitoring period. We selected an April 2–3, 2010 event for detailed analysis and discussion because it demonstrates a typical flooding response, was simultaneously monitored at RDP-1, RDP-2, and RDP-3 for water quality parameters, isotope geochemistry, and major and trace elemental composition, and had baseflow and event water components that were well characterized and substantially different. The hydrologic, isotopic, and geochemical responses are shown in Fig. 2.

#### 3.1.1 Rainfall totals and isotopic composition

During the April 2–3, 2010 event, which was proceeded by 0.69 cm of rain on March 28, 2010, a total of 1.06 cm of rain fell at Lambert-St. Louis International Airport (NOAA, 2015; Fig. 2a), while 1.24 and 1.40 cm fell at our rain

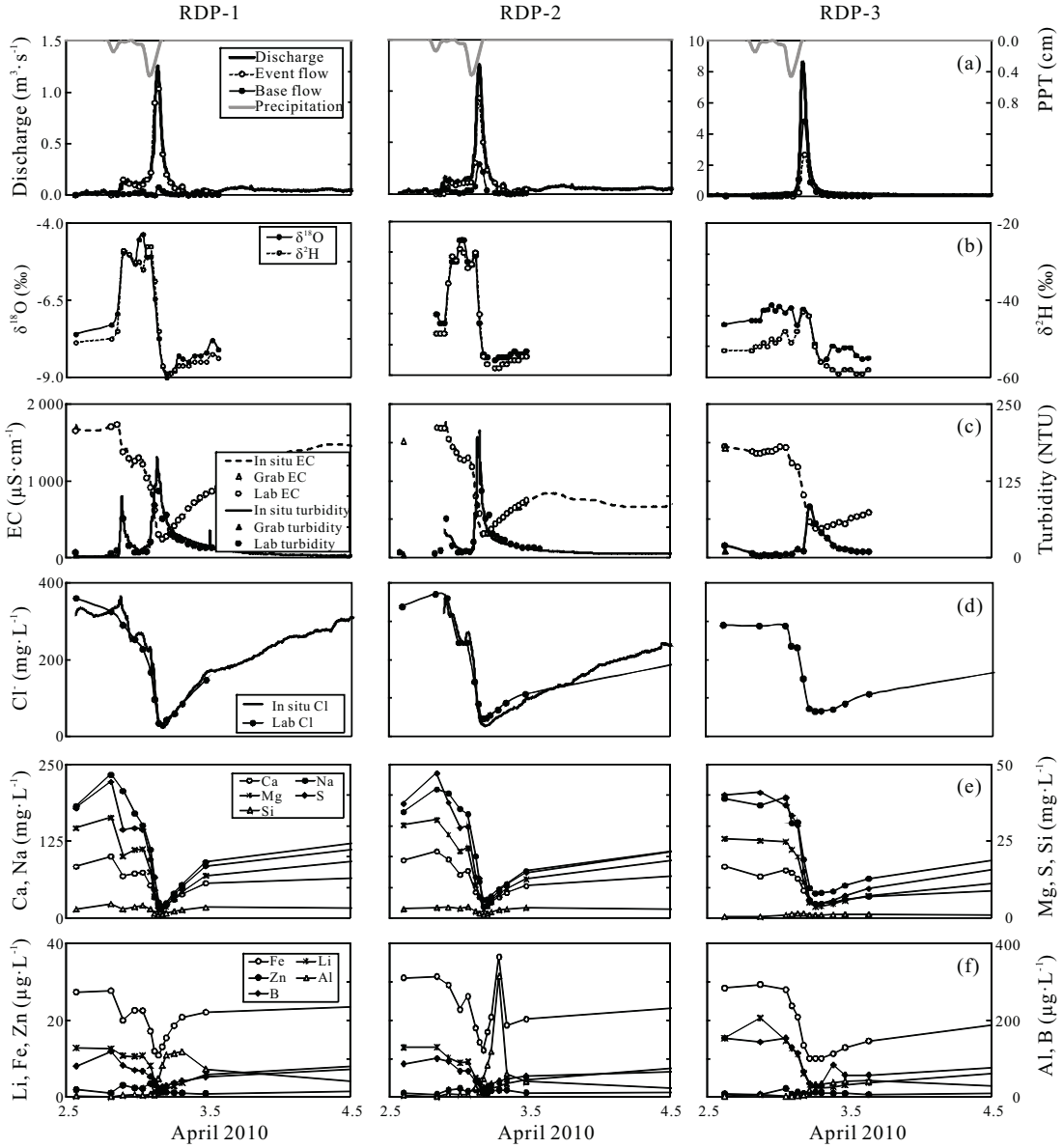


**Figure 2.** The hydrologic, isotopic, and geochemical responses of the Upper River des Peres sites (i.e., RDP-1, RDP-2, and RDP-3) to the April 2–3, 2010 rainfall events. Results include: (a) total discharge, baseflow and event water component hydrographs (determined by isotopic hydrograph separation), and precipitation totals; (b) laboratory $\delta^{18}O$ and $\delta^{2}H$ measurements; (c) field and laboratory EC and turbidity measurements; (d) field and laboratory $Cl^-$ measurements; (e) laboratory measurements of the major elements Ca, Na, Mg, S, and Si; and (f) laboratory measurements of selected minor elements Li, Fe, Zn, Al, and B. All parameters are on the same scale except for discharge at RDP-3. All data are from this study except for total discharge at RDP-3 (USGS, 2015b) and hourly rainfall (NOAA, 2015).

gauges in University City and Ladue, respectively. Official data from Lambert-St. Louis International Airport show that the rain fell in two increments, 0.20 cm from 20:00–22:00 on April 2, and 0.86 cm from 0:00–3:00 on April 3 (NOAA, 2015). Samples collected at University City show that the first increment had higher $\delta^{18}O$ and $\delta^{2}H$ values (0.69 cm; -4.2‰ and -25‰) than the second (0.55 cm; -9.1‰ and -62‰). At Ladue, a single composite sample for the April 2–3 rainfall had similar $\delta^{18}O$ and $\delta^{2}H$ values (-6.9‰ and -42‰) as the weighted averages for the two University City subsamples (-6.7‰ and -41‰).

### 3.1.2 Stream hydrologic and isotopic response

Following the first rainfall event on April 2, discharge at RDP-1 increased 0.1 $m^3s^{-1}$ from baseflow levels; however, the response was broad and flattened with no distinct discharge maximum (Fig. 2a). A larger, more typical discharge response followed the second increment of rainfall. In detail, discharge increased rapidly and was followed by a gradual recession to pre-event discharge rates (Table 1; Fig. 2a). Discharge was not gauged at RDP-2, but given its proximity to the RDP-1 station, the RDP-1 discharge measurements are a close approximation. RDP-3 also exhibited an initially broad and flattened response to the first rainfall event (Fig. 2a). However, the rapid onset of peak flow in response to the second rainfall event occurred 30 minutes later than peak flow at RDP-1 (Table 1). Additionally, it took 5 h longer to achieve near-baseflow conditions at RDP-

3 (Table 1; Fig. 2a). The RDP-3 catchment area is ~8 times larger than RDP-1 (Table 1; Fig. 1), so the peak discharge is proportionally larger.

Large, transient changes to the stream $\delta^{18}O$ and $\delta^{2}H$ composition occurred at all sites during the flood event (Table 1; Fig. 2b). The first, isotopically enriched rainfall event resulted in $\delta^{18}O$ and $\delta^{2}H$ enrichment in stream waters prior to peak discharge. However, after the second rainfall event and during peak discharge, floodwaters became depleted. The isotopic behavior at RDP-1 and RDP-2 were similar, but the response at RDP-2 was more attenuated than RDP-1; RDP-3 had the least variable isotopic response (Table 1; Fig. 2b). These isotopic data were used to calculate the component hydrographs so that we could address hyporheic flow along each of the channel reaches. The component hydrographs featured characteristics similar to the total discharge hydrograph, including steep rising limbs that peaked at approximately the same time as the total discharge peak, followed by a gradual recession to pre-event conditions (Fig. 2a). Importantly, the component hydrographs also revealed that the total baseflow fraction increased downstream from RDP-1 to RDP-3 (Table 1; Fig. 2a). Additionally, we observed the minimum baseflow contribution to stream flow shortly after peak discharge at all the sites. RDP-1 had a baseflow minimum of 0%, but minimum baseflow contributions increased downstream to 17% at RDP-3 (Table 1).

### 3.1.3 Stream geochemical response

The overall appearance of the April 2010 storm chemographs is similar between sites; however, in general, the largest geochemical perturbations occurred in the lined, upstream reach and became less pronounced downstream in the unlined reach. Because of equipment malfunctions at the RDP-3 site, water quality parameters were not monitored continuously in the field, but EC, turbidity, and $Cl^-$ were measured in the laboratory for samples automatically collected in the field.

Discharge pulses (Fig. 2a) were accompanied by concomitant decreases in EC (Fig. 2c). Prior to the flooding event, EC was highest at RDP-1 and decreased downstream (Table 1). "First flushing" events, in which EC could increase by up to 80 $\mu S \cdot cm^{-1}$, were associated with the rising limb of the hydrograph. This effect was largest at RDP-1 and decreased downstream (Fig. 2c). The first flushing events were followed by a general decline in EC that was punctuated by transient EC minima. The EC minima were most common at RDP-1 (i.e., 5 occurrences), followed by RPD-2 (i.e., 3 occurrences), then RDP-3 (i.e., 1 occurrence, though we recognize that the less frequent sampling routine at this site may have missed additional minima; Fig. 2c). The reduction of floodwater EC toward minimum values was observed on the recessional limb of the second, larger event for each site. The absolute minimum EC value recorded increased downstream by to almost 170 $\mu S \cdot cm^{-1}$ (Table 1).

Flooding at each of the sites resulted in a temporary increase in turbidity (Fig. 2c). In detail, two turbidity peaks (maximum values are 99 and 163 NTU) were observed at RDP-1 that coincided with the rising limbs of the flood hydrographs. The first turbidity perturbation at RDP-2 was not fully captured by the continuous monitoring equipment, but the maximum value measured in the laboratory measurements was 64 NTU. During the second event at RDP-2, the turbidity reached a maximum of 203 NTU; 20% higher than the response at RDP-1. Unlike the upstream sites, RDP-3 had only one small turbidity peak (i.e., 109 NTU).

Correlation analyses for discharge, isotopes, EC, pH, turbidity, and 27 elements and ions are given in Table S1. These analyses demonstrate the clustering of certain variables with correlation coefficients of variables in the same group above 0.65 or below -0.65. Elements tended to cluster into three categories: elements that correlate with EC, elements that correlate with parameters other than EC and EC-group elements, and elements that show no correlation with any parameter.

Concentrations of the baseflow-associated major elements and ions Ca, K, Mg, Na, S, and $Cl^-$, and minor elements B, Ba, Co, Fe, Ga, Li, Ni, Rb, and Sr are positively correlated with EC and each other, while Mo and Si are weakly correlated with many of the EC-group elements (Table S1). Like EC, the EC-group elements feature small concentration increases that coincide with the rising limb of the hydrograph (i.e., first flush events; Figs. 2d–2f). The continuous $Cl^-$ data provides the clearest example of this first flush behavior as well as transient minima patterns similar to those observed in EC (Fig. 2d). After the first flush, major element concentrations decreased to their lowest values concurrently with, or up to 80 min after, peak discharge (Figs. 2d–2f). The largest concentration reductions (>80%) were observed in the major ions ($Cl^-$; Fig. 2d) and elements (Ca, Mg, and Na; Fig. 2e), which had high pre-storm concentrations. After dilution, concentrations slowly returned to pre-event levels. The major element chemographs were similar between RDP-1 and RDP-2; however, concentrations were, on average, ~5% lower at RDP-2 before the discharge event and ~10% higher during peak discharge. At RDP-3, pre-event major element concentrations were typically 10%–25% lower than at RDP-1 and RDP-2, but during peak flow were 10%–30% higher (Figs. 2d and 2e). Additionally, most trace element concentrations were lower throughout the discharge event at RDP-3 compared to the upstream sites. However, B and Li were significantly higher at RDP-3 than at RDP-2 (i.e., B=35% higher, $p<0.01$; Li=20% higher, $p=0.02$; Fig. 2f). A notable exception to the EC-group elements' general behavior is the Fe chemograph at RDP-2 (Fig. 2f). Here, Fe levels declined during the rising limb of the flood hydrograph but increased 3-fold on the recessional limb, which is significantly higher than the Fe concentrations at RDP-1 ($p=0.02$). RDP-2's Fe response was not correlated with turbidity (Table S1).

Several other elements showed more complex behavior and correlated with other constituents, but not EC (Table S1). For example, Al exhibited a strong positive correlation with Pb. Al (Fig. 2f) and Pb (data not shown) concentrations were initially low (<2 and <0.2 $\mu g \cdot L^{-1}$, respectively) at all the sites, but increased during the recessional limb of the event before returning to near ambient levels; this behavior was most pronounced at RDP-2. Like the Fe response at RDP-2, Al and Pb do not show a strong correlation with turbidity (Table S1). Additionally, a weak, positive correlation was observed between Cu and Zn (Table S1); both Cu (data not shown) and Zn (Fig. 2f) had concentration maxima on the rising limb of the hydrograph and decreased after peak discharge. Cu and Zn

were highest at the upstream site and decreased downstream. Finally, a third group of parameters including discharge, pH, turbidity, Cd, Mn, $NH_4^+$-N, $NO_3^-$-N, and total $PO_4^{3-}$ did not correlate with each other or any other parameter (Table S1). Nonetheless, the nutrients (i.e., $NH_4^+$-N, $NO_3^-$-N, and total $PO_4^{3-}$) from this group had higher concentrations at RDP-1 than RDP-2 ($p$=0.05).

### 3.2 Diurnal and Seasonal Behavior

Many of the continuously monitored parameters showed both diurnal and seasonal variations (Fig. 3). Discharge was highly variable over the study period and could increase substantially following rainfall events or experience small diurnal fluctuations (especially in the summer months). Flow always increased downstream as watershed area increased (Table 1). Expectedly, isotope values were typically enriched during the summer and depleted during the winter (Fig. 3a). In contrast to the highly variable isotopic response between sites during transient storm events (Fig. 2b), the long-term average isotopic compositions were similar between sites (i.e., -7.0‰ to -7.3‰ for $\delta^{18}O$ and -47‰ to -49‰ for $\delta^2H$; Fig. 3a).

Diurnal and seasonal fluctuations in temperature were least pronounced at RDP-1 (SD=8.3 ºC) because a large, erosional plunge pool (~1 m deep during normal flow conditions) helped attenuate variations in air temperature (Table 1; Fig. 3b). However, temperature variability declined in the unlined channel reach between RDP-2 (SD=9.7 ºC) and RDP-3 (SD=9.5 ºC). For all sites, pH was highest in the spring and decreased in the summer (Fig. 3c). The pH also fluctuated daily, with highs during the day and lows at night. Both the average pH and the

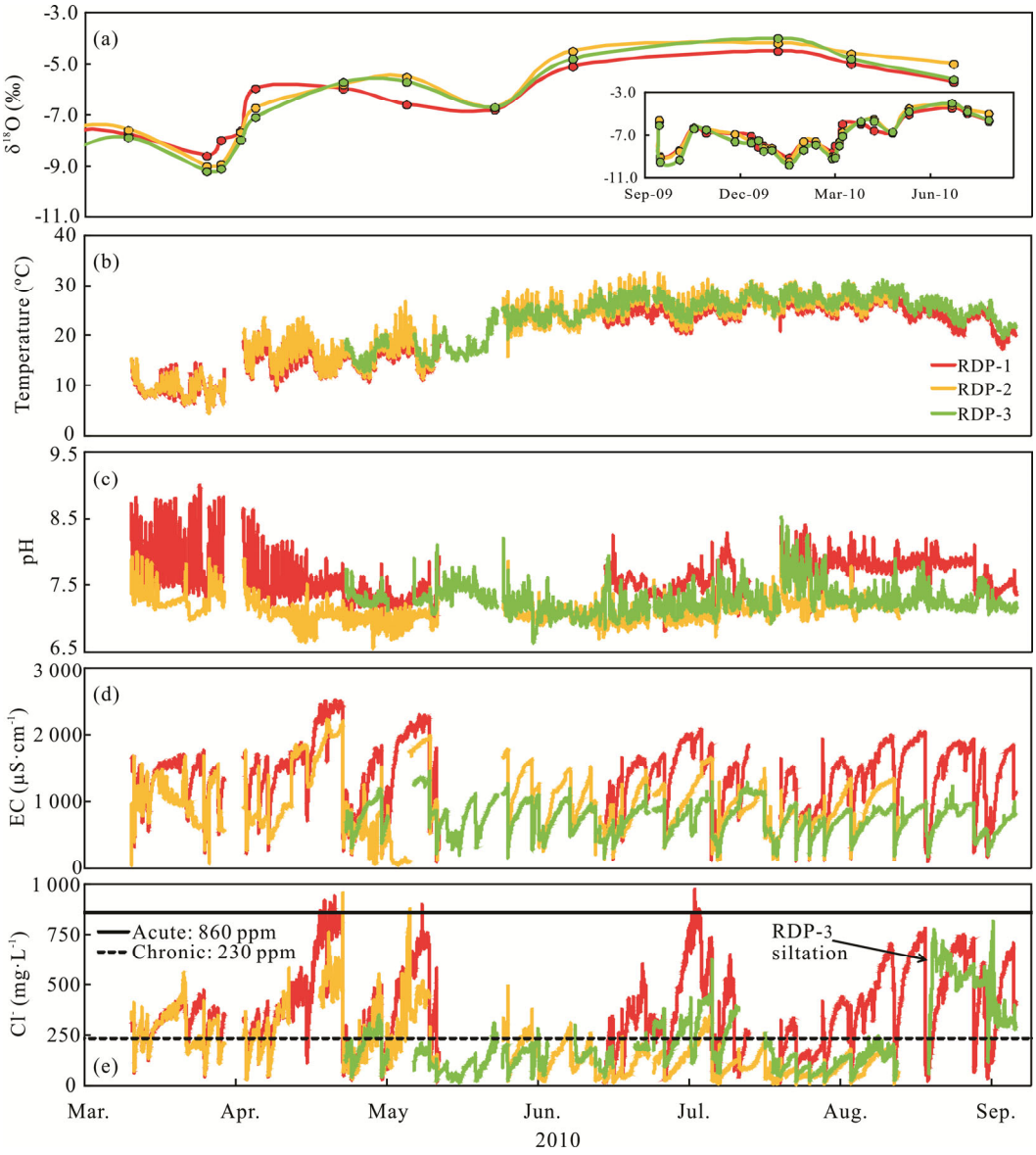


**Figure 3.** Selected seasonal data for RDP-1 (red), RDP-2 (yellow), and RDP-3 (green) including: grab sample data for (a) $\delta^{18}O$ and continuous monitoring data for (b) temperature, (c) pH, (d) EC, and (e) $Cl^-$. Note that the $Cl^-$ concentrations remain above regulatory limits for chronic $Cl^-$ contamination (230 mg·L$^{-1}$) even in the spring and summer months, and on several occasions exceed the acute $Cl^-$ contamination level (860 mg·L$^{-1}$). A portion of data is missing for RDP-1 when the continuous monitoring sensor was damaged by water leaks. Additionally, anomalously high $Cl^-$ levels were observed at RDP-3 when a portion of the monitoring equipment was buried in silt deposits.

amplitude of diurnal fluctuations were lower at RDP-2 than RDP-1 and RDP-3 (Table 1; Fig. 3c). In contrast, the DO ranged from 74.4% to 83.4% and increased downstream (Table 1).

EC (Fig. 3d) and $Cl^-$ (Fig. 3e) values were highest in March and decreased during the summer months. During summer low flow, EC in the catchment remained substantially higher than nearby rural watersheds that typically have values of ~200 $\mu S \cdot cm^{-1}$ (Hasenmueller and Criss, 2013b). Snow melt runoff measurements in the basin indicate that road salt is the dominant contributor to high EC, as melt runoff can have EC levels exceeding 36 000 $\mu S \cdot cm^{-1}$ and $Cl^-$ levels of almost 14 000 $mg \cdot L^{-1}$ (Hasenmueller and Criss, 2013a). Indeed, grab samples collected during our study indicate that winter $Cl^-$ levels were frequently elevated, reaching 1 400 $mg \cdot L^{-1}$; however, other studies in the River des Peres watershed indicate that peak $Cl^-$ levels are likely much higher (Hasenmueller, 2011; Shock et al., 2003). The $Cl^-$ concentrations at all three sites consistently exceeded the EPA chronic $Cl^-$ toxicity level (230 $mg \cdot L^{-1}$) during low flow periods, and, on several occasions in the late spring, RDP-1 and RDP-2 exceeded the EPA acute $Cl^-$ toxicity limit of 860 $mg \cdot L^{-1}$ (Fig. 3e). Average EC consistently decreases downstream, dropping almost 90 $\mu S \cdot cm^{-1}$ across the short distance of 320 m between RDP-1 and RDP-2 and 150 $\mu S \cdot cm^{-1}$ between RDP-2 and RDP-3 (Table 1). However, RDP-1's EC was up to 600 $\mu S \cdot cm^{-1}$ higher than RDP-2 during low flow conditions (Fig. 3d). This variation decreased and reversed during flooding: generally EC at RDP-2 was 50 $\mu S \cdot cm^{-1}$ higher than RDP-1 (Table 1; Figs. 2c and 3d). Likewise, average $Cl^-$ was highest at RDP-1 and decreased downstream almost 30 $mg \cdot L^{-1}$ at RDP-3 (Table 1). The $Cl^-$ at RDP-1 also remained higher during low flow conditions and lower during high flow conditions compared to the downstream sites (Table 1; Fig. 3e).

Total N-species were similar between RDP-1 and RDP-2 (i.e., $NH_4^+$-N and $NO_3^-$-N; $p$=0.75; Table 1); however higher $NH_4^+$-N was observed at RDP-1 ($p$=0.04), while $NO_3^-$-N was higher at RDP-2 ($p$=0.05). This is likely the result of the increasing DO downstream (Table 1) oxidizing $NH_4^+$-N to $NO_3^-$-N. The lowest concentrations of N-species were observed at RDP-3. Total P, on the other hand, consistently decreased downstream (Table 1). Finally, the average *E. coli* levels also declined from RDP-1 to RDP-3 (Table 1).

### 3.3 Spatial Trends in Geochemistry for an Unlined Reach

Geochemical surveys along the reach between RDP-1 and RDP-2 in November 2014 and March 2015 showed a decreasing trend in EC, $Cl^-$, and pH as the southwest branch of the Upper River des Peres flows from the concrete-lined channel through the unlined channel (Fig. 4). In November, EC decreased by 11% from 1 873 $\mu S \cdot cm^{-1}$ at RDP-1 to 1 670 $\mu S \cdot cm^{-1}$ at RDP-2. In March, the average EC was 70% higher than in November because of recent road salt application. Nevertheless, EC decreased from 3 025 $\mu S \cdot cm^{-1}$ at RDP-1 to 2 936 $\mu S \cdot cm^{-1}$ at RDP-2. The general EC decline downstream in both November and March was punctuated by sharp, localized decreases (Fig. 4a). The $Cl^-$ concentrations were only measured in November because of equipment problems during the March sampling event. Nonetheless, in November, $Cl^-$ fell from 571 to 547 $mg \cdot L^{-1}$ along the reach (Fig. 4b). The spatial $Cl^-$ data exhibited a few localized concentrations spikes up to 631 $mg \cdot L^{-1}$, which mostly occurred within 60 m of RDP-1. The pH decreased from 7.86 to 7.58 in November, while in March the pH was almost a full unit higher (Fig. 4c). Nevertheless, the decreasing trend in pH along the reach was still observed in March (i.e., 8.84 to 8.34).

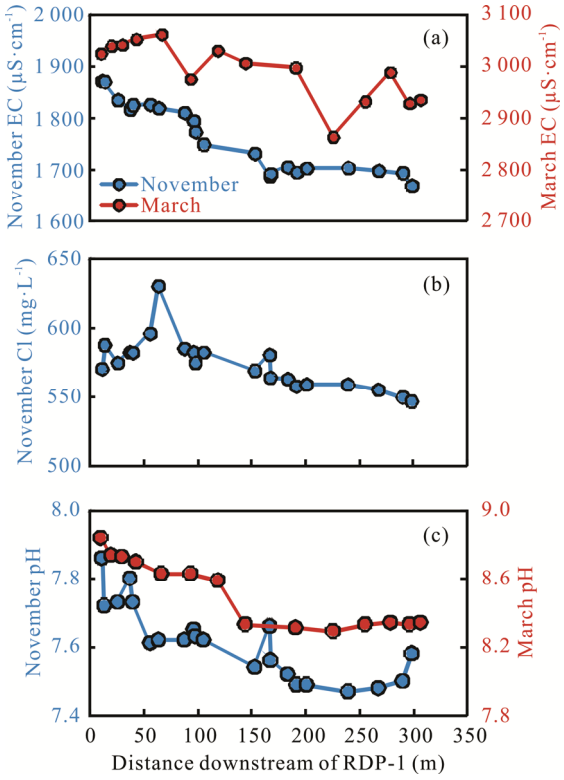


**Figure 4.** Geochemical variations measured with handheld meters along the reach between RDP-1 and RDP-2. The (a) EC, (b) $Cl^-$, and (c) pH were measured on November 12, 2014 (blue), but only (a) EC and (c) pH were measured on March 11, 2015 (red) due to problems with the $Cl^-$ sensor. Observe that all of these parameters tend to decrease downstream in the unlined reach.

## 4 DISCUSSION

We found that channelization in an urban stream, particularly the construction of cement-lined channels, reduces groundwater contributions to stream flow and amplifies geochemical variability. Below the lined reach of the southwest branch of the Upper River des Peres, the more natural channel bed maintains groundwater-surface water interactions along the hyporheic zone. The physical disconnection that occurs in the lined reach is exemplified by the stream's more variable short- (i.e., flood chemographs and diurnal response) and long-term (i.e., seasonal) geochemical behavior. Here, we interpret these hydrologic and geochemical variations in relation to mechanisms that reduce hyporheic exchange: channel linings reduce groundwater contributions to streams.

### 4.1 Impact of Channel Linings on the Hydrologic Response

In minimally impacted watersheds, as rainfall infiltrates the soil, it causes an increase in head that is hydraulically

transmitted through the phreatic zone, resulting in increased groundwater discharge to surface streams (Criss and Winston, 2008a, b; Criss, 2003, 1997). Indeed, for natural systems, baseflow is generally the largest contributor to discharge during floods (Waddington et al., 1993; Freeze and Cherry, 1979). However, the Upper River des Peres Basin exhibits rapidly changing hydrographs with higher peak flows than forested watersheds in the area (Frederickson and Criss, 1999). The short lag time at RDP-1 and RDP-3 (<2 h; Table 1) indicates rapid transmission of event water to the channel that does not mimic diffusive flow and shows that the hydrologic response is impacted by urban land use. Thus, it is important to determine the extent to which baseflow contributions are further reduced in urban streams by channel linings.

The southwest branch of the Upper River des Peres is entirely cement-lined above RDP-1, while below this site a more natural channel is present in a wooded area (Fig. 1). Isotopic hydrograph separations show that the unlined channel between RDP-1 and RDP-2 preserves groundwater recharge to the stream. In particular, groundwater contributions, measured for 10 storm events, were an average of 16% higher at RDP-2 than RDP-1 during flooding events (Table 1). This contribution is variable, however, and groundwater contributions were only 8% higher at RDP-2 compared to RDP-1 during the April 2010 event. Baseflow contributions increased by an average of 3% between RDP-2 and RDP-3, but again these contributions vary substantially between storms. Indeed, during the April 2010 event the baseflow component was two times higher at RDP-3 compared to RDP-2 (Table 1).

Interestingly, while isotopic variability in response to transient storm events dramatically decreased downstream from RDP-1 to RDP-3 (Fig. 2b), there was less variability between sites (i.e., SD=1.3%–1.6‰ for $\delta^{18}O$ and SD=7.8%–8.9‰ for $\delta^{2}H$) over longer periods (Fig. 3a). For our study, we could not deploy monitoring equipment in the cement-lined reach above RDP-1 because the water was too shallow; rather, we had to install the equipment in the deeper plunge pool just below the lined reach. It is possible that some of the long-term isotopic variability at RDP-1 was muted because of water storage in the plunge pool, as was the case for temperature variability. Nevertheless, seasonal isotopic variability was highest upstream and lowest downstream.

### 4.2 Geochemical Differences in Lined and Unlined Channels

The geochemical differences between RDP-1 and RDP-2, located only 320 m apart, also reveal that stream channel linings can appreciably limit baseflow contributions. The EC and EC-group elements in particular exemplified these changes. During flooding, we observed up to 80-min differences in concentration minima for elements associated with EC (i.e., baseflow-associated elements), showing that many of these elements have complex pathways during discharge events. Additionally, EC and EC-group elements generally increased downstream during peak discharge, as the higher baseflow component buffered the effect of the influx of dilute event water. The observed transient minima in EC are likely the result of the rapid delivery of event water in the upstream cement-lined channel. Fewer transient minima and smoother reductions in EC were observed at the downstream sites, probably due to buffering of event water pulses by the larger baseflow component. Finally, at the beginning of flooding events, we often observed spikes in EC and EC-group elements during first flush events. This behavior is typically attributed to the high pollutant loads at the onset of stormwater runoff (Lee et al., 2002). The magnitude of the first flush is reduced downstream because stormwater runoff constitutes a lower proportion of flow at downstream, unlined sites.

Interestingly, Winston and Criss (2004) observed strikingly different behavior for several EC-group elements, including B, Co, Fe, and Ni, in the flooding response of Bluegrass Spring, a karst spring 26 km southwest of the Upper River des Peres. In particular, B and Fe were negatively correlated with EC at Bluegrass Spring, while Co and Ni showed no correlation with EC. Hasenmueller and Criss (2013a) found that elevated B levels throughout the Upper River des Peres watershed were due to non-point source contributions from municipal drinking water used for lawn irrigation. Thus, we surmise that the correlation between EC and B in this watershed is the result of anthropogenic activities that increase the concentrations of B in baseflow. Elevated levels of Co and Ni likely also result from anthropogenic sources, but specific sources were not identified in this study.

Higher pollutant loads may also control the behavior of Fe in the watershed, as Fe concentrations tended to display first flushing behavior on the rising limb of the hydrograph, followed by decreasing concentrations during the recessional limb, after which Fe slowly recovered to pre-event levels. At RDP-2, however, Fe concentrations rose 3-fold during the recessional limb of the hydrograph. High Fe concentrations are often associated with high sediment loads (Steuber and Criss, 2005). Indeed, RDP-2 resides in a more natural streambed with a greater potential for channel erosion than RDP-1. The highest turbidity levels during the April 2010 event were observed at RDP-2 (Fig. 1), where highly erosive water leaving the artificial channel could enhance suspended sediment loads along the more natural channel. Interestingly, despite large stretches of unlined channel, the turbidity is lowest at RDP-3. We speculate this is either due to decreasing water velocity along the unlined reach between RDP-2 and RDP-3 (where channel roughness is higher) or contributions of less turbid water from the main stem and unnamed tributary. Nevertheless, the Fe maximum at RDP-2 does not coincide with either of the turbidity maxima (Table S1), and thus, it is unlikely that small clay particles are responsible for higher Fe values. The Fe trend at RDP-2 could represent pulses of acidic soil water from the nearby municipal park, as evidenced by generally lower pH values at RDP-2 (Table 1; Figs. 3c and 4c).

Al and Pb, which are also often associated with higher suspended loads (Winston and Criss, 2004), do not show a strong correlation with turbidity during the April 2010 event at any of the sites. Therefore, they are unlikely to be associated with suspended clay particles. It is possible that Al and Pb behavior may also be due to pulses of acidic soil water. While the correlation coefficients between pH and Al and Pb are low (Table S1), the highest Al and Pb concentrations occur at the same time as the lowest pH values, and possibly represent a

threshold response. Acidic rain waters could leach these elements from the soil (Winston and Criss, 2004), but more work is needed to verify this relationship. Cu and Zn concentrations tend to be higher on the rising limb of the storm hydrograph and therefore, are likely associated with the event water and its path to the channel.

Diurnal oscillations in various parameters also establish that there are increasing baseflow contributions along the stream. As mentioned above, daily temperature oscillations are low at RDP-1 because of the plunge pool, but decrease between RDP-2 and RDP-3. Daily changes in pH (Fig. 3c) as well as DO and N-species (data not shown) at the sites are related to changes in aquatic biological activity throughout the day (i.e., the dominance of photosynthesis during the day and respiration at night). These oscillations increase in amplitude in the summer months when these organisms are most active. The pH is least variable at RDP-2 and increases at RDP-3, probably because more shading near the RDP-2 site leads to lower aquatic photosynthesis levels. The EC (Fig. 3d) and $Cl^-$ (Fig. 3e) also increased slightly during the day, probably because of higher evaporation rates. This result is corroborated by small, daily variations in discharge where discharge decreases during the day and increases at night (data not shown). These effects are most pronounced in the summer months when evaporation rates are highest. Our data show that the amplitude of diurnal oscillations in EC (Fig. 3d) and $Cl^-$ (Fig. 3e) as well as DO and N-species diminish downstream due to baseflow contributions and hyporheic mixing.

On seasonal timescales, EC and associated elements (with the exception of B and Li), turbidity, nutrients, and *E. coli* levels decline downstream while DO levels rise (Table 1). These seasonal trends indicate that dilute groundwater contributions increase along the unlined reach. Interestingly, the seasonal behavior of turbidity at RDP-2 differs from its flooding response: we observe the highest turbidity levels only during transient storm events (Fig. 2c) when channel erosion can occur and intermediate turbidity levels during low flow conditions.

### 4.3 Spatial Trends in Hyporheic Zone Flow

Data collected along two detailed traverses between RDP-1 and RDP-2 show that EC, $Cl^-$ and pH systematically decrease downstream (Fig. 4). The progressive dilution observed along this reach implies a minimum increase in baseflow of 11% on November 15, 2014, and 3% on March 11, 2015. These additions agree well with the 8% increase observed during the April 2010 event and with the average baseflow increase of 16% observed for all storm events for which isotopic hydrograph separations were conducted. Nevertheless, it is likely that the actual increase in baseflow between these two sites is substantially higher than these estimates because the EC of the groundwater (baseflow) end-member must be higher than zero. Data of Hasenmueller and Criss (2013b) show that the EC of local groundwater ranges from 600 to 1 200 $\mu S \cdot cm^{-1}$; therefore, the increase in baseflow between RDP-1 and RDP-2 was likely closer to 16%–30% in November and to 4%–5% during March. However, because our March survey followed multiple applications of winter road salt, the EC of shallow groundwater was probably higher than in November. Consequently, our March estimates of EC in the groundwater end-member could be too low because the properties of baseflow are seasonally variable.

Like EC, the November $Cl^-$ concentrations tended to decrease downstream, though this trend was punctuated by a few sharp increases. Shock et al. (2003) showed that winter EC spikes in the Upper River des Peres closely followed road salt applications, implying a relationship between EC and $Cl^-$. Interestingly, our EC and $Cl^-$ data had only a weak relationship ($R^2$=0.44, $n$=21) within this particular reach. However, the higher correlation between EC and $Cl^-$ observed by Shock et al. (2003) is likely the result of elevated EC and $Cl^-$ values observed in their study (up to 10 000 $\mu S \cdot cm^{-1}$ and 3 000 $mg \cdot L^{-1}$, respectively), which anchor the correlation. Because we were unable to capture the post-salting season $Cl^-$ trend due to equipment problems, further investigation of the temporal behavior of EC and $Cl^-$ is necessary.

The gradual decrease in pH along the reach that was observed in both November and March indicates the addition of acidic soil water and/or shallow groundwater. Stream waters were almost a full pH unit higher in March than in November, likely due to the decreased biological activity in the catchment over the winter.

We suggest that the segments along the study reach that show smooth decreases in EC and the other parameters feature the diffuse inflow of either shallow groundwater or soil water that are contributed to the channel via the hyporheic zone (Haria et al., 2012). However, the largely smooth changes in these EC values were punctuated by several abrupt decreases that roughly coincided between the November and March sampling events, though the magnitude of change was greater in March (Fig. 4a). These abrupt decreases could represent concentrated inputs of dilute groundwater entering the channel. This shows that hyporheic flow generally increases along the unlined reach but is heterogeneous in space and time. It is possible that hyporheic flows were even absent along short segments of unlined channel, though the overall trends in EC, $Cl^-$, and pH indicate generally that baseflow tends to increase downstream.

It is important to note that increased baseflow contributions and the corresponding water quality improvements between RDP-1 and RDP-2 occur in spite of similar land use and nearly identical percentages of impervious land cover and length of roads within the drainage areas (Table 1). These similarities suggest that the geochemical variations between these sites reflect inhibited hyporheic exchange in the lined reach above RDP-1 and the existence of a hyporheic zone between RDP-1 and RDP-2. Between RDP-2 and RDP-3, the percentage of impervious surface area becomes even larger, so our results indicate that channel engineering, rather than land use, is a dominant control on baseflow input to the stream channel. In short, our geochemical traverses, combined with our isotopic evidence, show that hyporheic flow is inhibited along lined channel reaches.

## 5 CONCLUSIONS

Comparison of lined and unlined reaches of the Upper River des Peres shows that channelization and streambed linings significantly disrupt groundwater-surface water interactions along the hyporheic zone. Although the catchments have

similar land use, the unlined, more natural channel reaches have high baseflow contributions that foster good water quality and low geochemical variability. In contrast, the lined reaches exhibit lower water quality, increased geochemical variability, and higher event flow fractions during flooding. Quantifying the loss of hyporheic flow along lined channels is critical for predicting hydrologic and geochemical changes to urban streams over daily to seasonal timescales. Baseflow contributions help buffer extreme chemical variations in urban streams, which has important implications for urban stream management and ecosystem health.

## ACKNOWLEDGMENTS

This work was partially supported by a USEPA subcontract from the Watershed Management Plan Development Grant Program through the Missouri Department of Natural Resources to the University City Department of Public Works (No. G06-NPS-18). ICP-OES and ICP-MS analyses were performed at the Nano Research Facility (NRF) of Washington University, a member of the National Nanotechnology Infrastructure Network (NNIN), which is supported by the National Science Foundation (No. ECS-0335765). We thank two anonymous reviewers for constructive comments that helped improve this manuscript. The final publication is available at Springer via http://dx.doi.org/10.1007/s12583-016-0632-5.

**Electronic Supplementary Material:** Supplementary material (Table S1) is available in the online version of this article at http://dx.doi.org/10.1007/s12583-016-0632-5.

## REFERENCES CITED

Boulton, A. J., Findlay, S., Marmonier, P., et al., 1998. The Functional Significance of the Hyporheic Zone in Streams and Rivers. *Annual Review of Ecology and Systematics*, 29(1): 59–81. doi:10.1146/annurev.ecolsys.29.1.59

Buffington, J. M., Tonina, D., 2009. Hyporheic Exchange in Mountain Rivers II: Effects of Channel Morphology on Mechanics, Scales, and Rates of Exchange. *Geography Compass*, 3(3): 1038–1062. doi:10.1111/j.1749-8198.2009.00225.x

Bukaveckas, P. A., 2007. Effects of Channel Restoration on Water Velocity, Transient Storage, and Nutrient Uptake in a Channelized Stream. *Environmental Science & Technology*, 41(5): 1570–1576. doi:10.1021/es061618x

Criss, R. E., 1997. New Formulation for the Hydrograph, Time Constants for Stream Flow, and the Variable Character of Base Flow. *Transactions American Geophysical Union*, 78: 317

Criss, R. E., 1999. Principles of Stable Isotope Distribution. Oxford University Press, Oxford. 254

Criss, R. E., 2003. Hydrograph for Small Basins Following Intense Storms. *Geophysical Research Letters*, 30(6): 1314–1318. doi:10.1029/2002gl016808

Criss, R. E., Winston, W. E., 2008a. Discharge Predictions of a Rainfall-Driven Theoretical Hydrograph Compared to Common Models and Observed Data. *Water Resources Research*, 44(10): W10407. doi:10.1029/2007wr006415

Criss, R. E., Winston, W. E., 2008b. Properties of a Diffusive Hydrograph and the Interpretation of Its Single Parameter. *Mathematical Geosciences*, 40(3): 313–325. doi:10.1007/s11004-008-9145-9

Fetter, C. W., 2001. Applied Hydrogeology, 4th Ed. Prentice Hall, Upper Saddle River. 598

Frederickson, G. C., Criss, R. E., 1999. Isotope Hydrology and Residence Times of the Unimpounded Meramec River Basin, Missouri. *Chemical Geology*, 157(3/4): 303–317. doi:10.1016/s0009-2541(99)00008-x

Freeze, R. A., Cherry, J. A., 1979. Groundwater. Prentice-Hall, Englewood Cliffs, NJ. 604

Gooseff, M. N., LaNier, J., Haggerty, R., et al., 2005. Determining In-Channel (Dead Zone) Transient Storage by Comparing Solute Transport in a Bedrock Channel-Alluvial Channel Sequence, Oregon. *Water Resources Research*, 41(6): W06014. doi:10.1029/2004wr003513

Hach, 2005a. Method 8206, Chloride, Mercuric Nitrate, in Digital Titrator Model 16900 Manual. Hach Company, Loveland, CO, USA

Hach, 2005b. Method 8038, Nitrogen, Ammonia: Nessler Method. Hach Company, Loveland, CO, USA

Hach, 2005c. Method 10020, Nitrate: Chromotrophic Acid Method. Hach Company, Loveland, CO, USA

Hach, 2005d. Method 8048, Phosphorus: Reactive (Orthophosphate) Method. Hach Company, Loveland, CO, USA

Hach, 2005e. Method 8190, Phosphorus: Total Digestion. Hach Company, Loveland, CO, USA

Hancock, P. J., 2002. Human Impacts on the Stream-Groundwater Exchange Zone. *Environmental Management*, 29(6): 763–781. doi:10.1007/s00267-001-0064-5

Haria, A. H., Shand, P., Soulsby, C., et al., 2012. Spatial Delineation of Groundwater-Surface Water Interactions through Intensive In-Stream Profiling. *Hydrological Processes*, 27(4): 628–634. doi:10.1002/hyp.9551

Harrison, R. W., 1997. Bedrock Geologic Map of the St. Louis 30′×60′ Quadrangle, Missouri and Illinois. U.S. Geological Survey Miscellaneous Investigation Series Map I-2533, Scale 1 : 100 000

Hasenmueller, E. A., 2011. The Hydrology and Geochemistry of Urban and Rural Watersheds in East-Central Missouri: [Dissertation]. Washington University, St. Louis. 382

Hasenmueller, E. A., Criss, R. E., 2013a. Multiple Sources of Boron in Urban Surface Waters and Groundwaters. *Science of the Total Environment*, 447: 235–247. doi:10.1016/j.scitotenv.2013.01.001

Hasenmueller, E. A., Criss, R. E., 2013b. Geochemical Techniques to Discover Open Cave Passage in Karst Spring Systems. *Applied Geochemistry*, 29: 126–134. doi:10.1016/j.apgeochem.2012.11.004

Hinkle, S. R., Duff, J. H., Triska, F. J., et al., 2001. Linking Hyporheic Flow and Nitrogen Cycling near the Willamette River—A Large River in Oregon, USA. *Journal of Hydrology*, 244(3/4): 157–180. doi:10.1016/s0022-1694(01)00335-3

Lau, J. K., Lauer, T. E., Weinman, M. L., 2006. Impacts of Channelization on Stream Habitats and Associated Fish Assemblages in East Central Indiana. *The American Midland Naturalist*, 156(2): 319–330. doi:10.1674/0003-

0031(2006)156[319:iocosh]2.0.co;2

Lee, J. H., Bang, K. W., Ketchum, L. H., et al., 2002. First Flush Analysis of Urban Storm Runoff. *Science of the Total Environment*, 293(1–3): 163–175. doi:10.1016/s0048-9697(02)00006-2

Lutzen, E. E., Rockaway, J. D. Jr., 1989. Engineering Geologic Map of St. Louis County, Missouri. Missouri Department of Natural Resources, Open File Map 89-256-EG

Metropolitan St. Louis Sewer District (MSD), 2015. Metropolitan St. Louis Sewer District: Sewer Overflows [2015-12-11]. http://www.stlmsd.com/sites/default/files/education/448847.PDF

National Oceanic and Atmospheric Administration (NOAA), 2015. National Weather Service (NWS) Weather: NWS [2015-12-11]. http://www.weather.gov

Rivett, M. O., Ellis, P. A., MacKay, R., 2011. Urban Groundwater Baseflow Influence upon Inorganic River-Water Quality: The River Tame Headwaters Catchment in the City of Birmingham, UK. *Journal of Hydrology*, 400(1/2): 206–222. doi:10.1016/j.jhydrol.2011.01.036

Ryan, R. J., Welty, C., Larson, P. C., 2010. Variation in Surface Water-Groundwater Exchange with Land Use in an Urban Stream. *Journal of Hydrology*, 392(1/2): 1–11. doi:10.1016/j.jhydrol.2010.06.004

Shock, E. L., Carbery, E., Noblit, N., et al., 2003. Water and Solute Sources in an Urban Stream, River des Peres, St. Louis, Missouri. In: Criss, R. E., Wilson, D. E., eds., At the Confluence: Rivers, Floods, and Water Quality in the St. Louis Region. Missouri Botanical Garden Press, St. Louis, Missouri. 150–160

Sklash, M. G., Farvolden, R. N., 1979. The Role of Groundwater in Storm Runoff. *Journal of Hydrology*, 43(1–4): 45–65. doi:10.1016/0022-1694(79)90164-1

Stueber, A. M., Criss, R. E., 2005. Origin and Transport of Dissolved Chemicals in a Karst Watershed, Southwestern Illinois. *Journal of the American Water Resources Association*, 41(2): 267–290. doi:10.1111/j.1752-1688.2005.tb03734.x

U.S. Census, 2010. Population Density Date: 2010 U.S. Census [2014-12-15]. http://2010.census.gov/2010census

U.S. Environmental Protection Agency (EPA), 1990. Method 200.7: Determinations of Metals and Trace Elements in Water and Wastes by Inductively Coupled Plasma-Atomic Emission Spectrometry. U.S. Environmental Protection Agency, Revision 3.0

U.S. Environmental Protection Agency (EPA), 1994. Method 200.8: Determinations of Trace Elements in Waters and Wastes by Inductively Coupled Plasma-Mass Spectrometry. U.S. Environmental Protection Agency, Revision 5.4

U.S. Geological Survey (USGS), 2015a. USGS Land Cover Institute (LCI): U.S. Land Cover [2014-12-15]. http://landcover.usgs.gov/uslandcover.php

U.S. Geological Survey (USGS), 2015b. USGS Real-Time Data for Missouri: USGS Real-Time Data for Missouri [2014-12-15]. http://waterdata.usgs.gov/mo/nwis/rt

Vaughn, D. M., 1990. Flood Dynamics of a Concrete-Lined, Urban Stream in Kansas City, Missouri. *Earth Surface Processes and Landforms*, 15(6): 525–537. doi:10.1002/esp.3290150605

Waddington, J. M., Roulet, N. T., Hill, A. R., 1993. Runoff Mechanisms in a Forested Groundwater Discharge Wetland. *Journal of Hydrology*, 147(1–4): 37–60. doi:10.1016/0022-1694(93)90074-j

White, D. S., 1993. Perspectives on Defining and Delineating Hyporheic Zones. *Journal of the North American Benthological Society*, 12(1): 61–69. doi:10.2307/1467686

Winston, W. E., Criss, R. E., 2004. Dynamic Hydrologic and Geochemical Response in a Perennial Karst Spring. *Water Resources Research*, 40(5): W05106. doi:10.1029/2004wr003054

Wondzell, S. M., Swanson, F. J., 1999. Floods, Channel Change, and the Hyporheic Zone. *Water Resources Research*, 35(2): 555–567. doi:10.1029/1998wr900047